

05,10

## Heating of magnetic powders in the ferromagnetic resonance mode at a frequency of 8.9 GHz

© S.V. Stolyar<sup>1,2</sup>, O.A. Lj<sup>1,2</sup>, E.D. Nikolaeva<sup>1</sup>, N.M. Boev<sup>2,3</sup>, A.M. Vorotynov<sup>3</sup>, D.A. Velikanov<sup>3</sup>, R.S. Iskhakov<sup>3</sup>, V.F. Pyankov<sup>1</sup>, Yu.V. Knyazev<sup>3</sup>, O.A. Bayukov<sup>3</sup>, A.O. Shokhrina<sup>1,2</sup>, M.S. Molokeev<sup>2,3</sup>, A.D. Vasiliev<sup>2,3</sup>

<sup>1</sup> Krasnoyarsk Scientific Center of the Siberian Branch of the Russian Academy of Sciences, Krasnoyarsk, Russia

<sup>2</sup> Siberian Federal University, Krasnoyarsk, Russia

<sup>3</sup> Kirensky Institute of Physics, Federal Research Center KSC SB, Russian Academy of Sciences, Krasnoyarsk, Russia

E-mail: stol@iph.krasn.ru

Received April 17, 2023

Revised April 17, 2023

Accepted May 11, 2023

Nickel ferrite nanoparticles 4 nm in size were synthesized by chemical deposition. Subsequent annealing at  $T = 700^\circ\text{C}$  for 5 h led to an increase in the particle size to 63 nm. The Mössbauer spectra and the frequency-field dependences of ferromagnetic resonance have been measured. It has been shown that freshly prepared powders are superparamagnetic at room temperature. The kinetic dependences of the heating of nanoparticles in the ferromagnetic resonance mode at a frequency of 8.9 GHz were measured. It was found that the maximum rate of temperature increase in this mode for a ferromagnetic powder is an order of magnitude greater than for the superparamagnetic state (1.2 and 0.13 K/s, respectively). The latter is determined by the saturation magnetization of the studied powders.

**Keywords:** ferromagnetic resonance, superparamagnetic powders, relaxation frequency, frequency-field dependence, heating of powders.

DOI: 10.21883/PSS.2023.06.56109.21H

### 1. Introduction

The field of application of magnetic nanoparticles is constantly expanding. In biomedicine, there are already proven approaches to the practical applications of magnetic nanoparticles. In magnetic hyperthermia, an alternating magnetic field ( $H \sim 100\text{ Oe}$ ,  $f \sim 100\text{ kHz}$ ) in particle remagnetization processes performs local heating of biological tissues [1]. As a rule, magnetite-maghemite particles or ferrites based thereon are the objects of research for this area. Metal oxides and ferromagnetic metal nanoparticles based on 3-d metals [2] alloys are used less frequently. Biocompatible coatings such as chitosan, polyethylene glycol, tetraethylorthosilicate (TEOS) and 3-aminopropyltriethoxysilane (APTES) etc. are used to reduce the toxicity of magnetic nanoparticles [2–6].

Research into the efficiency of particle heating for magnetic hyperthermia applications has been conducted on both dry powder systems and magnetic liquids. In papers [3,7–13], the dependences of the heating temperature of nickel ferrite particles on their magnetic properties, method of production and external conditions have been studied. The re-magnetization mechanisms of magnetic nanoparticles (hysteresis loss, Néel rotation, Brownian rotation) leading to their heating are primarily determined by their size [3,9,14,15]. The heating rates during nanoparticle

remagnetization are determined by the magnitude and frequency of the field used and are  $\sim 1\text{ K/s}$  [9].

Extending the frequency range of hyperthermia, another possible way of heating can be pointed out: its realization via ferromagnetic resonance (FMR) [7,16,17].

The instantaneous value of the magnetization vector  $\mathbf{M}$  in a magnetic field  $\mathbf{H}_{\text{eff}}$  is determined by the Landau-Lifshitz-Gilbert equation:

$$\dot{\mathbf{M}} = -\gamma\mathbf{M} \times \mathbf{H}_{\text{eff}} - \frac{\gamma\alpha}{M}\mathbf{M} \times (\mathbf{M} \times \mathbf{H}_{\text{eff}}),$$

where  $\gamma$  — gyromagnetic ratio,  $\alpha$  — damping parameter. The damping parameter is related to the relaxation time  $\tau$ , i.e. the time required to damp the precession of the magnetization vector, by the following relation [18]:

$$\tau^{-1} = \omega_r = \alpha\gamma H_{\text{eff}},$$

$\omega_r$  — relaxation frequency. If a high-frequency microwave field with frequency  $\omega$  and amplitude  $h$ , orthogonal to the external field  $H$ , acts on the magnetization  $M$  besides the DC field  $H$ , resonance absorption of microwave energy by the ferromagnet (FMR) is possible. The magnetic susceptibility  $\chi = m/h$  is the complex value  $\chi = \chi' + \chi''$ . The imaginary component of the magnetic susceptibility  $\chi''$  near the frequency  $\omega$ , at which the microwave energy

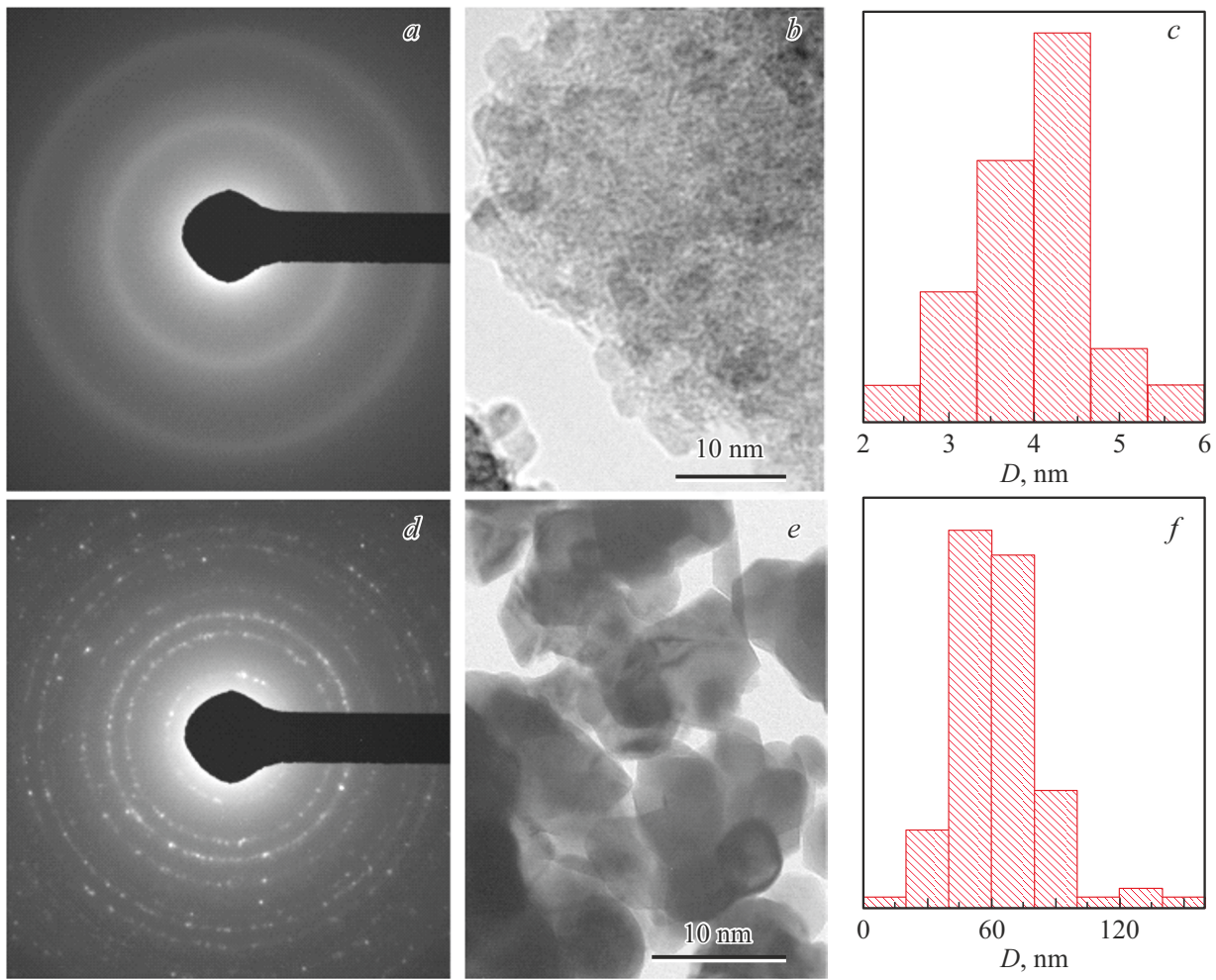


**Figure 1.** Electron diffraction pattern and microphotographs of nickel ferrite particles before (a,b) and after (d,e) annealing, (c,f) — particle size distribution.

is absorbed by the ferromagnet has a maximum value. At frequencies  $\omega > \omega_r$ , there is resonant absorption of microwave energy  $\alpha \sim 0.1 \ll 1$ . At  $\omega < \omega_r$ , the relaxation mechanisms of  $\alpha > 1$  absorption act. In FMR mode, for the case of a spherical ferromagnet  $\chi''_{\text{res}} \approx \frac{1}{2} \frac{\gamma' M_S}{\alpha f}$ , where  $\gamma' = \gamma/2\pi \approx 2.8 \text{ MHz/Oe}$ . The energy absorption of a spherical particle of volume  $V$  per unit time is determined by the expression  $Q = \omega(V/2)\chi''h^2$ .

Assuming that all of the microwave energy absorbed by the nanoparticle goes into heating it, the heat balance equation can be written down:  $Cm\Delta T = Q\Delta t$ , which allows the relations between temperature rise rate and particle characteristics to be established

$$dT/dt = h^2\gamma'M_S/4C\rho\alpha,$$

where  $\rho$  — density,  $C$  — specific heat capacity.

The proposed paper is devoted to the study of FMR heating of magnetic nickel ferrite powders produced by chemical deposition.

## 2. Experiment procedure

Nickel ferrite nanoparticles were prepared by chemical deposition followed by a five-hour annealing at 700°C [19]. Microphotographs were taken with a Hitachi HT7700 transmission electron microscope. X-ray diffraction analysis was performed on a DX-2700BH, HAOYUAN,  $\lambda = 0.154 \text{ nm}$ . Mössbauer spectra of the studied samples were obtained on a MS-1104Em spectrometer in transmission geometry with radioactive source  $\text{Co}^{57}(\text{Rh})$  at 300 K. The nanoparticles temperature was measured with a T-type thermocouple with copper and constantan electrodes placed in a waveguide electron paramagnetic resonance (EPR) spectrometer SE/X-2544 (Radiopan) X-band at 8.9 GHz (the magnetic field magnitude is determined with the built-in NMR magnetometer with an accuracy of  $10^{-2} \text{ Oe}$ , the error in frequency determination is 100 kHz). When placing the thermocouple in the resonator (without powder) with microwave pumping and a magnetic field sweep from 0 to 5 kOe, the thermocouple did not register any temperature change. The frequency-field dependencies of the fabricated

powders were studied with a broadband ferromagnetic resonance spectrometer at 300 K. Magnetization measurements were made on a vibrating magnetometer.

### 3. Results

Fig. 1 shows images of ferrite particles taken with a transmission electron microscope. Before annealing (Fig. 1, *b*), the particles had a close to spherical shape with an average particle size of  $4.0 \pm 0.7$  nm. After annealing (Fig. 1, *e*), the particle size increased significantly to  $63 \pm 22$  nm. Since the shape of the particles was not spherical, the particles were approximated by polygons to find the average particle size and the equivalent diameter of a circle of corresponding area was calculated.

Fig. 2 shows an X-ray diagram of the annealed sample, the insert shows an X-ray diagram of the original powder. After annealing, reflections from nickel ferrite and reflections from hematite  $\alpha\text{-Fe}_2\text{O}_3$  of low intensity are observed. The hematite phase proportion is 5%. The average crystal size was estimated using full-profile Rietveld refinement using the TOPAS 6 program. A correction for the instrumental broadening of the peaks is introduced with reference sample — Si. The calculated crystal size was  $75 \pm 15$  nm for the powder after heat annealing.

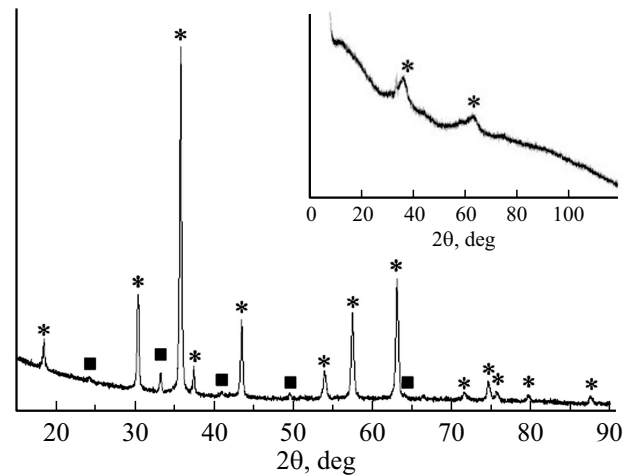
The saturation magnetization of the  $M_S$  powders was 5 emu/g at room temperature. After annealing, there was an increase in magnetization to 34 emu/g [19]. The value of  $M_S$  is consistent with results obtained by other authors [3].

Fig. 3 and 4 show the Mössbauer spectra of the original and annealed samples, respectively. The parameters of the spectra are given in Tables 1 and 2, respectively. The spectrum of the initial powders is a quadrupole doublet, indicating a superparamagnetic state of the particles. The spectrum of the annealed powders is a resolved sextet, indicating a magnetic-ordered state of iron magnetic moments. This is achieved by increasing the size of the nanoparticles compared to the unannealed sample.

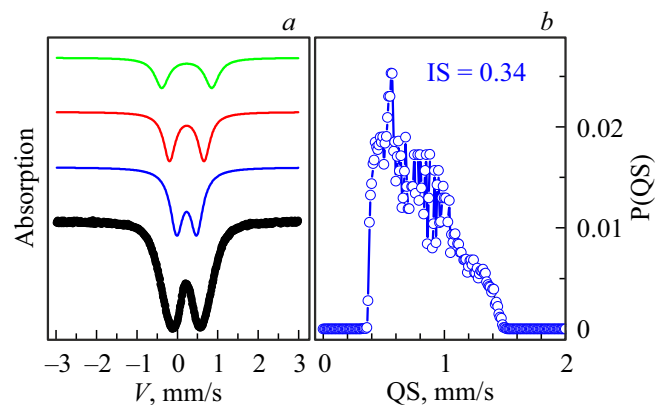
The spectrum decomposition results show that in addition to the spinel phase, the annealed sample contains a hematite phase with a proportion of 16%. The spinel part is represented by iron in tetrahedral and octahedral positions in the ratio A:B = 1.8:1.0. In unsubstituted magnetite, this ratio is 1.0:2.0, i.e. the substitution occurs at octahedral sites.

Fig. 5 shows the distribution of the microwave energy absorption spectra of the powders studied.

Fig. 6 shows frequency dependences of the real component of magnetic permeability  $\mu'$  at different DC magnetic field strengths  $H$  and dependence of resonant frequency on external field  $H$  determined by the real component of magnetic permeability  $\mu'$ . By approximating the dependence by a linear function  $f(H) = f_0 + (\gamma H)/2\pi$ , the gap value in the frequency-field dependence  $f_0$  as well as the value of the gyromagnetic ratio  $\gamma$  can be estimated. For freshly cooked powders  $f_0 = 0$  (superparamagnetic state),



**Figure 2.** Diffraction patterns of the annealed and the original (insert) samples. (\*) asterisks — peaks corresponding to the nickel ferrite structure, (■) squares — peaks corresponding to the hematite structure.



**Figure 3.** Mössbauer spectrum of a freshly prepared sample with treatment result (*a*) and probability distributions of quadrupole splitting in the sample (*b*).

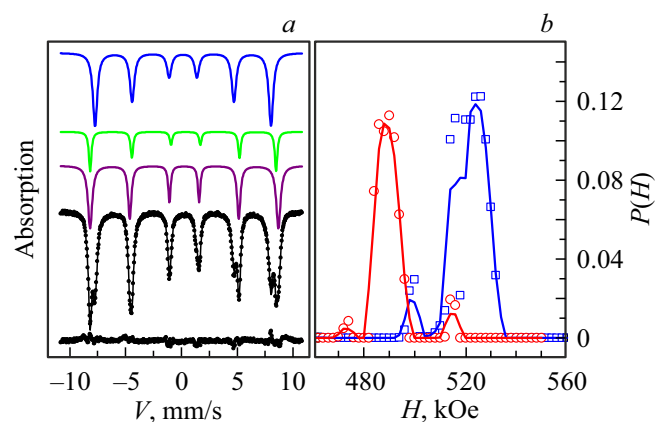


**Figure 4.** (*a*) Mössbauer spectrum of nickel ferrite after annealing at room temperature, lower diagram — error spectrum; (*b*) Probability distribution of hyperfine fields on iron nuclei in tetrahedral (red line) and in octahedral positions (blue line).

**Table 1.** Mössbauer spectrum parameters NiFe<sub>2</sub>O<sub>4</sub> without annealing

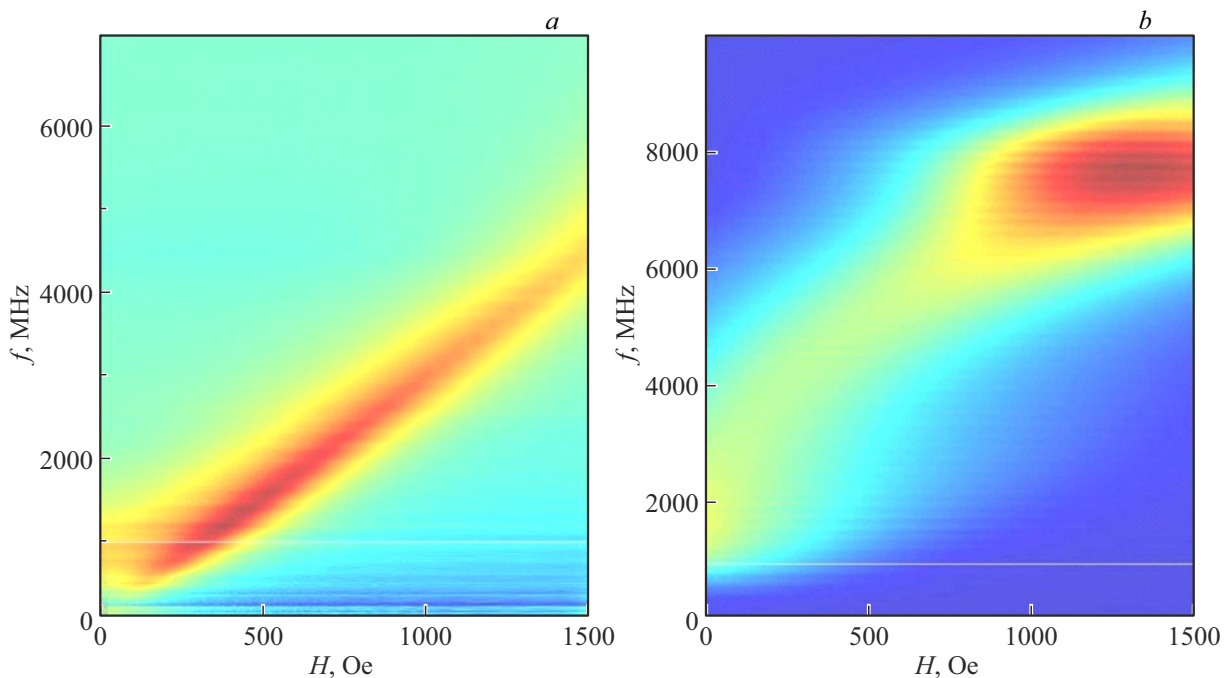
IS, mm/s ± 0.005	<i>H</i> , kOe, ±3	QS, mm/s ± 0.01	<i>W</i> , mm/s ± 0.01	<i>A</i> , a.u. ± 0.03	Site
0.34	–	1.26	0.40	0.21	Fe <sup>3+</sup> (B)
0.34	–	0.86	0.36	0.36	
0.34	–	0.49	0.37	0.42	Fe <sup>3+</sup> (A)

Note. IS — isomeric chemical shift with respect to  $\alpha$ -Fe, *H* — hyperfine field, QS — quadrupole splitting, *W* — line width, *A* — fractional position occupancy.

**Table 2.** Mössbauer spectrum parameters NiFe<sub>2</sub>O<sub>4</sub> after annealing

IS, mm/s ± 0.005	<i>H</i> , kOe, ±3	QS, mm/s ± 0.01	<i>W</i> , mm/s ± 0.01	<i>A</i> , a.u. ± 0.03	Site
0.378	519	0	0.23	0.30	(B)
0.268	486	0.002	0.43	0.54	[A]
0.373	517	–0.51	0.23	0.16	$\alpha$ -Fe <sub>2</sub> O <sub>3</sub>

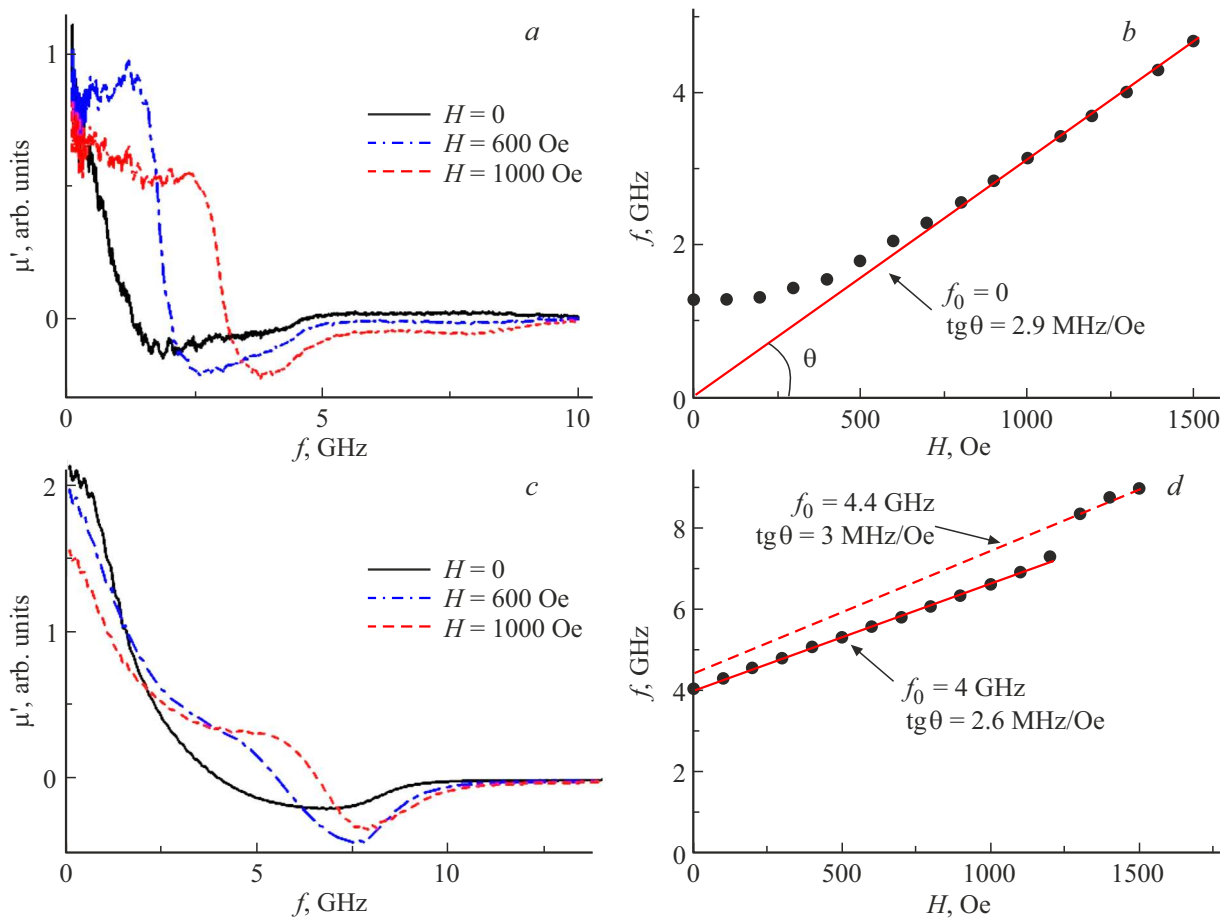
Note. IS — isomeric chemical shift with respect to  $\alpha$ -Fe, *H* — hyperfine field, QS — quadrupole splitting, *W* — line width, *A* — fractional position occupancy.

**Figure 5.** Energy absorption spectra at FMR of the original powders (*a*) and after annealing (*b*).

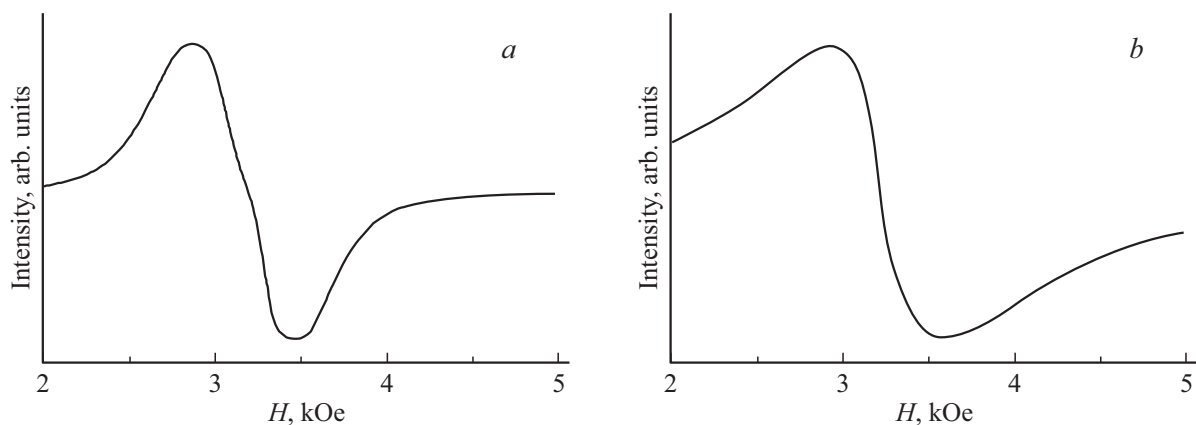
$\gamma = 1.8 \cdot 10^7$  Hz/Oe. After heat treatment of nickel ferrite powders  $f_0 \approx 4$  GHz,  $\gamma = 1.6 \cdot 10^7$  Hz/Oe. It should be noted that in paper [20], the frequency-field response of nickel ferrite powders with different particle sizes exhibited features similar to those we observed (Fig. 6, *b*). These features were not discussed by the authors.

Fig. 7 shows the FMR curves measured at 8.9 GHz and room temperature.

Fig. 8 shows the kinetic curves of powder temperature change during microwave pumping in a constant field of strength *H*. The highest heating was observed in the resonant field and amounted to  $\Delta T_{\max} = 5$  K for the initial powders and  $\Delta T_{\max} = 8$  K after annealing. The values are comparable to those obtained by [7], the authors of which obtained a heating value of 6.9 K for nickel ferrite particles at 3.0 GHz. If the magnetic field deviates from



**Figure 6.** Frequency dependences of the real part of the complex magnetic permeability and the dependence of the resonant frequency on the external field  $H$  for the initial (*a, b*) and annealed (*c, d*) samples.



**Figure 7.** FMR spectra ( $f = 8.9$  GHz) of the original powders (*a*) and after annealing (*b*).

the resonance value to one side or the other, the heating value  $\Delta T$  decreases (see Fig. 8, *a, b*). At  $H = 0$ , the effect is present: for initial powder  $\Delta T(H = 0) \approx 1$  K, after heat annealing  $\Delta T(H = 0) = 2$  K. Microwave energy absorption at  $H \rightarrow 0$  has previously been observed on various magnetic powder systems: on ferrites Co [21], on ferrites Ni-Zn [22], on metal alloys Co-Ni [23], on

superconductors [24], etc. The heating of our studied powder systems at  $H = 0$  (Fig. 8, *a, b*) can be explained, remaining within the framework of the FMR phenomenon, as microwave energy absorption by nanoparticles in their own internal field (anisotropy field), or by natural ferromagnetic resonance [18]. Any powder system is characterized by dispersion in crystallite sizes and orientations and hence

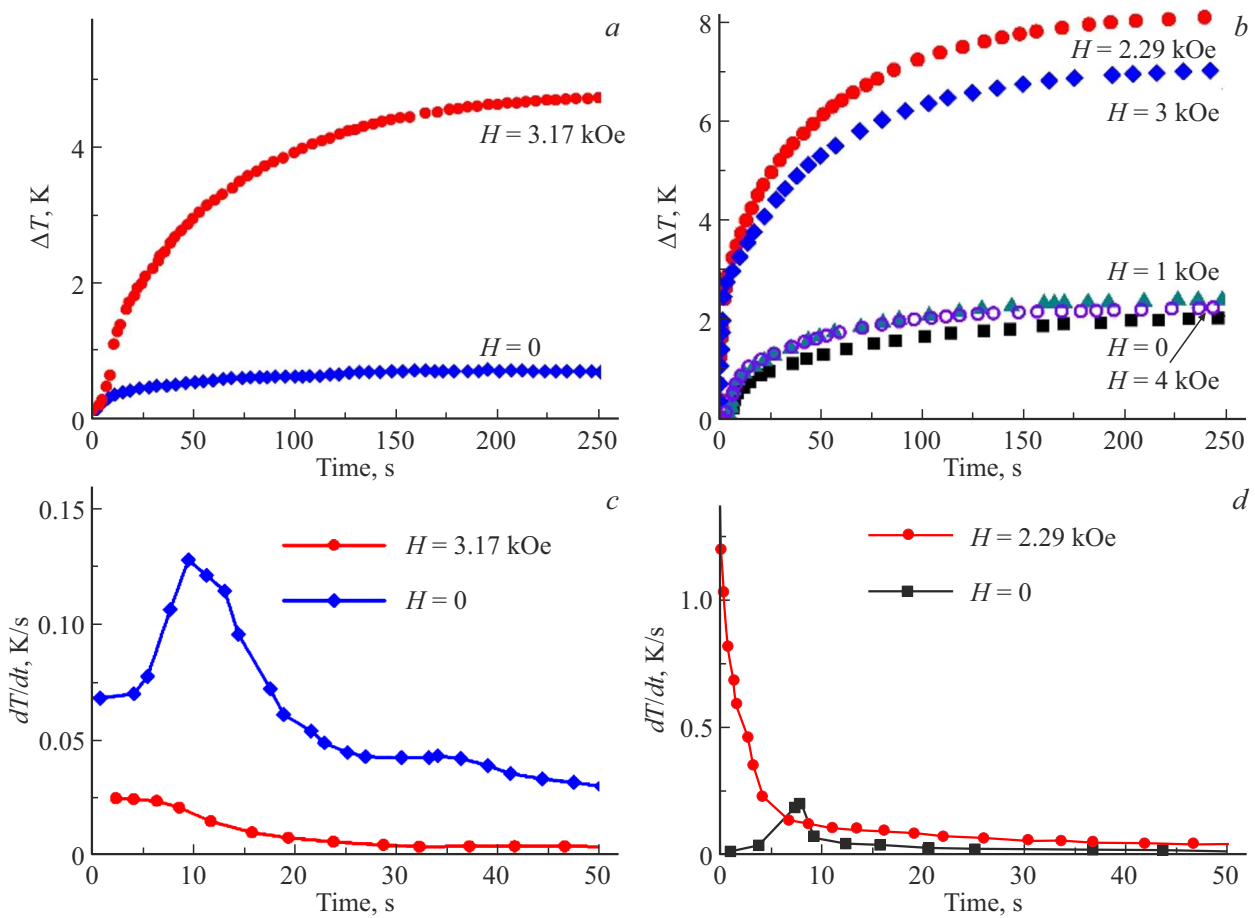


**Figure 8.** Dependences of temperature increment and heating rate on time for initial nickel ferrite (a, c) and after annealing (b, d).

dispersion in projections of internal fields in the direction perpendicular to the alternating magnetic field of the microwave. The latter provides a natural ferromagnetic resonance.

Fig. 8, c, d shows the temperature rise rates of powders during microwave absorption. In the resonant field, the heating rates differ by an order of magnitude (0.13 and 1.2 K/s, respectively).

#### 4. Discussion

Our experiments demonstrate that in the microwave absorption mode, the temperature rise rate  $dT/dt$  of heat treated powders (63 nm) is an order of magnitude greater than  $dT/dt$  of freshly made powders (4 nm) (0.13 and 1.2 K/s, respectively). The frequency-field relationships of superparamagnetic freshly cooked powders are well approximated by a line passing through the origin  $\omega_0 = \gamma H_{\text{eff}} = \gamma H$ ,  $H$  — external field (Fig. 6, b). At low frequencies, there is a deviation from the linear relationship  $\omega_0 = \gamma H$ , which can be related to an increase in the damping parameter  $\alpha$ . The resonant frequency of the FMR taking into account attenuation is defined by the expression

$\omega^2 = \omega_0^2(1 + \alpha^2)$ , where  $\alpha$  — the damping parameter [18]. The experimentally detected deviation of the resonant frequency from  $\omega_0$  allowed us to determine the damping parameter  $\alpha$  for freshly prepared superparamagnetic powder. The results are shown in Fig. 9. Since the relaxation frequency is proportional to the damping parameter and the field strength ( $\omega_r = \alpha \gamma H_{\text{eff}}$ ), approximating the dependence  $\alpha(1/\gamma H)$  by a linear function allows to find  $\omega_r$ . We obtained a value  $\omega_r = 1.3$  GHz (insert Fig. 9). In our view with  $\omega_r$ , there is a change in the mode of microwave energy absorption. At  $\omega > \omega_r$ , there is resonance absorption  $\alpha \sim 0.1 \ll 1$ . At  $\omega < \omega_r$ , the relaxation mechanisms of  $\alpha > 1$  absorption act. The observed by the authors of [20] specific features of the resonance frequency dependence on the field, apparently, can also be explained by a change in the microwave energy absorption mode and estimate the relaxation frequency to be 4–6 GHz.

For the frequency-field dependence of heat-treated nickel ferrite powders, a linear dependence is observed (Fig. 6, d), indicating a resonant mode of microwave energy absorption „of ferromagnetic“ powders at  $\alpha \sim 0.1 \ll 1$ . The specific feature on the frequency-field dependence of these powders at  $f = 8$  GHz, consisting in an abrupt decrease of the effective field  $H_{\text{eff}} = 2\pi f_0/\gamma + H$ , may be related

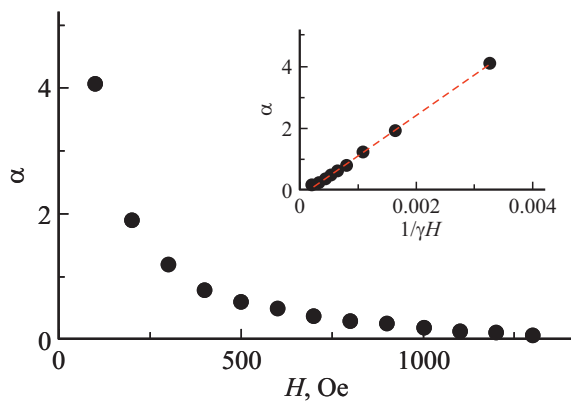


**Figure 9.** Dependence of the damping parameter  $\alpha$  on the magnitude of the constant external field. Insert — dependence  $\alpha(1/\gamma H)$  and its straight line approximation.

to the heterophasy of heat-treated powders. The ferrite powder after annealing contains the  $\alpha\text{-Fe}_2\text{O}_3$  phase as an impurity (approx. 10%), so the size of the hematite particles should be smaller than the nickel ferrite particles. The decrease in effective field  $H_{\text{eff}}$  with decreasing microwave frequency can be attributed to the transition of hematite particles to a superparamagnetic state. The relations between the blocking temperature  $T_B$  and the frequency used in the experiment  $f$  is given by the Néel–Brown expression:  $KV/T_B k_B = \ln(f_m/f)$ , where  $f_m$  — relaxation frequency, which for single-domain particles is in the interval  $1\text{ GHz} < f_m < 10^4\text{ GHz}$ ,  $KV$  — magnetic anisotropy energy of the nanoparticle,  $k_B$  — Boltzmann constant. In our case, at  $f = 8\text{ GHz}$ ,  $T_B = 300\text{ K}$  (room temperature). Above  $8\text{ GHz}$ , hematite nanoparticles exhibit „ferromagnetic“ properties; below  $8\text{ GHz}$ , they become superparamagnetic. Another explanation for the discussed feature is possible: at  $8\text{ GHz}$  for the impurity phase nanoparticles  $\alpha\text{-Fe}_2\text{O}_3$ , the microwave energy absorption mechanism is changed, i.e. this frequency for  $\alpha\text{-Fe}_2\text{O}_3$  is a relaxation frequency.

We measured the thermal effect ( $\Delta T$ ) at  $8.9\text{ GHz}$ . At this frequency, irrespective of the size of the ferrite powders under study, the resonance mode of the microwave field energy absorption  $\alpha \sim 0.1 \ll 1$  is realized. If in the expression for the rate of temperature increase ( $dT/dt = h^2 \gamma' M_S / 4C\rho\alpha$ ), the dependence of heat capacity  $C$  and density  $\rho$  on powder particle size is neglected, the difference  $dT/dt$  between the initial and the heat-treated powders will be solely determined by the saturation magnetization. The measured values are  $5$  and  $34\text{ emu/g}$  at room temperature, which provides the observed rate changes  $dT/dt$ .

## 5. Conclusion

Nickel ferrite powders  $\text{NiFe}_2\text{O}_4$  size  $\sim 4\text{ nm}$  were produced by chemical deposition method. As a result of

the heat treatment at  $T = 700^\circ\text{C}$  for  $5\text{ h}$  the powder size increased to  $63\text{ nm}$ . X-ray diffraction analysis shows that the  $\alpha\text{-Fe}_2\text{O}_3$  phase is present as an impurity in the powders after heat treatment. The Mössbauer spectrum of the initial powders is characteristic of the superparamagnetic state of the particles. The spectrum of the annealed powders is a resolved sextet and along with the spinel phase,  $\alpha\text{-Fe}_2\text{O}_3$  phase is present with a fraction of  $16\%$ . The microwave absorption spectra of the initial superparamagnetic powders reveal a deviation from the linear dependence  $\omega_0 = \gamma H$ , which allowed the damping parameter  $\alpha$  and the relaxation frequency  $\omega_r = 1.3\text{ GHz}$  to be determined. In our view with  $\omega_r$ , there is a change in the mode of microwave energy absorption. At  $\omega > \omega_r$ , there is resonance absorption ( $\alpha \sim 0.1 \ll 1$ ). At  $\omega < \omega_r$ , the relaxation mechanisms of  $\alpha > 1$  absorption act. The FMR curves and particle temperature-time dependences of microwave field energy absorption at  $8.9\text{ GHz}$  have been studied. The greatest heating of the powders under study is observed at a DC magnetic field strength equal to the resonance strength. It is found that the maximum rate of temperature increase for annealed powder is an order of magnitude greater than for the superparamagnetic state ( $0.13$  and  $1.2\text{ K/s}$ , respectively). The effect detected is determined by the magnetization of the powders under study. Our research allows to recommend nickel ferrite particles as targets for resonant hyperthermia, if the problems of their cytotoxicity and delivery to the respective targets [25] are solved.

## Conflict of interest

The authors declare that they have no conflict of interest.

## References

- [1] A.S. Kamzin, D.S. Nikam, S.H. Pawar. FTT **59**, *1*, 149 (2017). (in Russian). 10.21883/ftt.2017.01.43966.185.
- [2] M. Peiravi, H. Eslami, M. Ansari, H. Zare-Zardini. J. Indian Chem. Soc. **99**, *1*, 100269 (2022). 10.1016/j.jics.2021.100269.
- [3] Seongtae Bae, Sang Won Lee, A. Hirukawa, Y. Takemura, Youn Haeng Jo, Sang Geun Lee. IEEE Trans Nanotechnol. **8**, *1*, 86 (2009). 10.1109/TNANO.2008.2007214.
- [4] K. Ohara, T. Moriwaki, K. Nakazawa, T. Sakamoto, K. Nii, M. Abe, Y. Ichiyanagi. AIP Adv. **13**, *2*, 025238 (2023). 10.1063/9.0000477.
- [5] W. Wu, Z. Wu, T. Yu, C. Jiang, W.-S. Kim. Sci. Technol. Adv. Mater. **16**, *2*, 023501 (2015). 10.1088/1468-6996/16/2/023501.
- [6] M. Shen, H. Cai, X. Wang, X. Cao, K. Li, S.H. Wang, R. Guo, L. Zheng, G. Zhang, X. Shi. Nanotechnology **23**, *10*, 105601 (2012). 10.1088/0957-4484/23/10/105601.
- [7] J.-H. Lee, Y. Kim, S.-K. Kim. Sci. Rep. **12**, *1*, 5232 (2022). 10.1038/s41598-022-09159-z.
- [8] S. Bae, S.W. Lee, Y. Takemura. Appl. Phys. Lett. **89**, *25*, 252503 (2006). 10.1063/1.2420769.
- [9] A. Tomitaka, H. Kobayashi, T. Yamada, M. Jeun, S. Bae, Y. Takemura. J. Phys.: Conf. Ser. 200. Institute of Physics Publishing (2010).

- [10] E. Umut, M. Coşkun, F. Pineider, D. Berti, H. Güngüneş. *J. Coll. Interface Sci.* **550**, 199 (2019). 10.1016/j.jcis.2019.04.092.
- [11] Ç.E. Demirci Dönmez, P.K. Manna, R. Nickel, S. Aktürk, J. van Lierop. *ACS Appl. Mater. Interfaces* **11**, 7, 6858 (2019). 10.1021/acsami.8b22600.
- [12] G. Stefanou, D. Sakellari, K. Simeonidis, T. Kalabaliki, M. Angelakeris, C. Dendrinou-Samara, O. Kalogirou. *IEEE Trans. Magn.* **50**, 12, 1 (2014). 10.1109/TMAG.2014.2345637.
- [13] O.M. Lemine, N. Madkhali, M. Hjiri, N.A. All, M.S. Aida. *Ceram. Int.* **46**, 18, 28821 (2020). 10.1016/j.ceramint.2020.08.047.
- [14] A.E. Deatsch, B.A. Evans. *J. Magn. Magn. Mater.* **354**, 163 (2014). 10.1016/j.jmmm.2013.11.006.
- [15] M.V. Lebedev. *Vestn. Permskogo un-ta. Fizika* **4**, 14 (2021). (in Russian). 10.17072/1994-3598-2021-4-14-20.
- [16] S.V. Vonsovsky. *Ferromagnitnyy rezonans. Yavleniye rezonansnogo pogloshcheniya vysokochastotnogo elektromagnitnogo polya v ferromagnitnykh veshchestvakh. Fiz.-mat. lit., M.* (1961). (in Russian).
- [17] N. Yoshikawa, T. Kato. *J. Phys.* **43**, 42, 425403 (2010). 10.1088/0022-3727/43/42/425403.
- [18] S. Krupička. *Physik der Ferrite und der verwandten magnetischen Oxide.* Vieweg+Teubner Verlag, Wiesbaden (1973).
- [19] S.V. Stolyar, O.A. Li, E.D. Nikolaeva, A.M. Vorotynov, D.A. Velikanov, Y.V. Knyazev, O.A. Bayukov, R.S. Iskhakov, V.F. Pyankov, M.N. Volochaev. *FMM* **124**, 2, 182 (2023). (In Russian).
- [20] P. Hernández-Gómez, J.M. Muñoz, M.A. Valente, C. Torres, C. de Francisco. *EPJ Web Conf.* **40**, 17003 (2013). 10.1051/epjconf/20134017003.
- [21] M.E. Mata-Zamora, H. Montiel, G. Alvarez, J.M. Saniger, R. Zamorano, R. Valenzuela. *J. Magn. Magn. Mater.* **316**, 2, e532 (2007). 10.1016/j.jmmm.2007.03.011.
- [22] R. Valenzuela, S. Ammar, F. Herbst, R. Ortega-Zempoalteca. *Nanosci. Nanotechnology Lett.* **3**, 4, 598 (2011). 10.1166/nnl.2011.1207.
- [23] G.V. Kurlyandskaya, S.M. Bhagat, C. Luna, M. Vazquez. *J. Appl. Phys.* **99**, 10, 104308 (2006). 10.1063/1.2191740.
- [24] V.V. Srinivasu, S.E. Lofland, S.M. Bhagat, K. Ghosh, S. Tyagi. *J. Appl. Phys.* **86**, 2, 1067 (1999). 10.1063/1.371146.
- [25] S.V. Stolyar, L.A. Chekanova, R.N. Yaroslavtsev, S.V. Komogortsev, Y.V. Gerasimova, O.A. Bayukov, M.N. Volochaev, R.S. Iskhakov, I.V. Garanzha, O.S. Kolovskaya, M.S. Bairmani, T.N. Zamay. *J. Phys. Conf. Ser.* **1399**, 2, 022026 (2019). 10.1088/1742-6596/1399/2/022026.

*Translated by Ego Translating*